Technical report: Exercise 3

N. Pham

For Problem 1, one-dimensional and two-dimensional diffraction patterns were generated, both in the near-field regime and the far-field regime. The relationships of aperture width and screen distance with central intensity and central width were modelled and confirmed physical theories. For Problem 2, the Monte Carlo method was successfully used to approximate the volumes of a hyperspheres for 2 to 10 dimensions. The error of the method is shown to vary with the inverse square root of the sample size for this type of pseudorandom Monte Carlo method. The quasi-Monte Carlo method was also employed to loosely demonstrate quicker convergence compared to the pseudorandom method.

I. PROBLEM 1: FRESNEL DIFFRACTION FROM AN APERTURE

A. Introduction

Problem 1 required evaluating integrals to model the phenomenon of diffraction. The situation consists of an aperture at a distance z away from a screen. Both the aperture and the screen are centred around $x = y = 0$. The aperture has width d_a and the screen has width d_s. The model assumes monochromatic light with a wavelength λ, or wavenumber k.

Part (a) asked to model 1D diffraction in the far-field approximation ($d_a \ll z$) using two different numerical methods—Simpson's method and the quadrature method. Part (b) asked to investigate the effect on varying z and d_a on the diffraction pattern in the far-field approximation, as well as observing the effects of near-field diffraction ($d_a \sim z$), and also observe the effects of the number of data points N (for Simpson's method) on the appearance of the diffraction patterns for both far-field and near-field. Part (c) changed the situation to two-dimensional and the diffraction effect on the screen was investigated in far-field and near-field approximations, for square and rectangular apertures. Finally, part (d) asked for a circular aperture and similarly investigate the visual effects as one went from near-field to far-field approximations.

B. Theory

A general integral to solve for Fresnel diffraction through an aperture in the x, y plane is given by:

$$E(x,y,z) = A \iint\limits_{\text{Aperture}} e^{\frac{ik}{2z}\left[(x-x')^2+(y-y')^2\right]} \, \mathrm{d}x \, \mathrm{d}y \quad (1)$$

where $A = \frac{kE_0}{2\pi k}$, and the origin $z = 0$ is taken at the aperture. $E(x, y, z)$ is the electric field at any given coordinate x, y, z on the screen. The intensity of the diffracted light is given by:

Quantity	Value
λ	$1 \times 10^{-6}\,\mathrm{m}$
d_a	$2 \times 10^{-5}\,\mathrm{m}$
z	$2 \times 10^{-2}\,\mathrm{m}$
d_s	$1 \times 10^{-2}\,\mathrm{m}$

Table I. Default parameters used in one-dimensional and two-dimensional far-field diffraction.

$$I(x,y,z) = \epsilon_0 c E(x,y,z) E^*(x,y,z) \quad (2)$$

C. Method

In part (a), the Euler's formula was used to split the one-dimensional Fresnel diffraction integral into real cosine and imaginary sine part. Then, using `scipy` built-in integration methods `scipy.integrate.simpson` and `scipy.integrate.quad` to evaluate the these two integrals, keeping d_s, d_a, λ and z the same. Then, the intensity is calculated once the electric field has been solved. The result of this is that both diffraction effects should be near identical. The parameters are stored in Table I.

For part (b), the symmetry of the situation was kept so that the width of the aperture increases and decreases in size while the centre is still positioned at $x = 0$. Two quantities were measured to investigate the effects of aperture width—the peak intensity of the central maximum and the width of the central maximum (2 times the distance from the central maximum to the first minima). The central width was calculated using `scipy.signal.argrelextrema()` to find local minima. The range of aperture widths used is from $1 \times 10^{-4}\,\mathrm{m}$ to $4 \times 10^{-5}\,\mathrm{m}$. Similarly, peak intensity and width of central maximum were also measured to investigate the effects of varying screen distance. The range of aperture widths used is from $5 \times 10^{-3}\,\mathrm{m}$ to $9 \times 10^{-2}\,\mathrm{m}$. For the Simpson's method, the number of sample points N was varied and its effect on the shape of the diffraction pattern observed. N values chosen were 3, 7, 11, 31, 51, 101, 201, 301, 401.

For part (c), Euler's formula was used again, but now to split the two-dimensional Fresnel integral into a real cosine and imaginary sine part. The aperture can be changed to be rectangular by scaling the y dimension by a factor of the x dimension. Then, using `scipy.integrate.dblquad`, the double integral was evaluated directly. The result is then produced as a `matplotlib` image. Furthermore, the simulation was run for the following z values to observe the difference between near-field and far-field effects: 2.5×10^{-5} m, 5×10^{-5} m, 7.5×10^{-5} m, 1×10^{-4} m, 1.5×10^{-4} m, 2×10^{-4} m, 2.5×10^{-4} m, and 3×10^{-4} m.

For part (d), the same method in part (c) is used. However, the limits in x are not constants (to depict squares or rectangles) but functions so that the aperture is now circular. The new x limits are $\pm\sqrt{r^2 - y^2}$.

D. Results & discussions

For part (a), the parameters chosen produce identical scatter plots. Additionally, time elapsed for each method was calculated with `time.perf_counter()`. The Simpson's method took 0.287 s while the quadrature method took longer at 0.418 s.

For part (b), 500 points were generated for each plot of of Fig. 2, which shows that increasing the aperture width increases the peak intensity of the central maximum and decreases the width of the central maximum. Assuming the relationship is $I_0 \propto d_a^m$, it is quadratic as m is the slope of the logarithmic plot on the left, which is 2.00 to 3 significant figures. This models the physical phenomenon wherein the light intensity which comes through the aperture and diffracted onto the screen is proportional to the square of the aperture width. Meanwhile, assuming the relationship is $\sin\theta \approx \theta \propto d_a^n$ (θ being the angular half-width), the width of the central maximum 2θ is inversely proportional to the aperture width, as the slope of the logarithmic plot on the right is $n = -1.00$ to 3 significant figures. This models the physical phenomenon where the angular half-width is given as $\theta \sim \lambda/d_a$.

Similarly, 500 data points were generated for Fig. 3, which shows that increasing the screen distance decreases the intensity of the central maximum and increases the width of the central maximum. Assuming the relationship is $I_0 \propto z^o$, it satisfies the inverse square law as o is the slope of the plot on the left, which is -2.00 to 3 significant figures. This models the physical phenomenon where the intensity of light follows the inverse square law $I \propto 1/z^2$ where z is the distance between the light source and the screen. Meanwhile, assuming the relationship is $\sin\theta \approx \theta \propto z^p$, the width of the central maximum 2θ is proportional to z as p is the slope of the plot on the right, which is 1.00 to 3 significant figures. This models the physical phenomena where from symmetry, one can deduce that $\theta \propto \lambda z/d_a$.

Next, far-field effects at different values of N (data points for the Simpson's method) were modelled (Fig. 4). Only the pattern for $N > 101$ correctly produces the pattern, as the next one at $N = 51$ (coloured purple), has a second unexpected maxima far away from the screen centre. These unaccounted-for maxima appear closer to the centre and more frequently as N decreases. The pattern does not 'improve' for $N > 101$, showing that there is a lower threshold for N in which the Simpson's method is able to produce an accurate integration.

Next, near-field effects were observed by decreasing the screen distance z to 3×10^{-3} m while increasing the aperture width d_a to 2×10^{-3} m, and decreasing the area of the screen to integrate over from -2×10^{-2} m to 2×10^{-2} m. The sample size N was also increased to 401 for Fig. 5. Whereas before, there was only one central maximum, the pattern now resembles sets of adjacent maxima of equal intensity at high intensities (the less-dense, tall peaks) to low intensities (flatter, highly-dense peaks). Observed would be dark and bright bands, whereas in the far-field approximation there would only be one central band.

In the far-field approximation, $N = 101$ seemed to be the lower-bound to produce an accurate diffraction pattern. In the near-field approximation, the moss-coloured pattern ($N = 401$) seen in Fig. 6 (the same in Fig. 5) differs from the grey-coloured pattern ($N = 301$), and successively lower N-patterns differ from the previous one. This shows that near-field diffraction produces a more challenging integration which requires more samples to accurately approximate. As most of the colour-coding of each N value can be seen on their own with few overlaps, the accuracy of the Simpson's method for lower N reduces significantly for near-field approximation.

For part (c), square and rectangular apertures were modelled for near and far-field effects (Fig. 7 and Fig. 8). This requires integrating Eq. 1 in two dimensions. To get the simulations to run for near-field, the screen size had to be reduced in order for the code to run in reasonable timescale. Additionally, there were also artefacts produced, as seen in Fig. 8 (top left and top right), which is potentially a loss of accuracy in `scipy.integrate.dblquad()` as the limits of integration (screen size) were still too large in these two simulations. Regardless, near-field effects were observed for screen distance z at 1×10^{-4} m and below, as arrays of bright and dark rectangular and squares can be

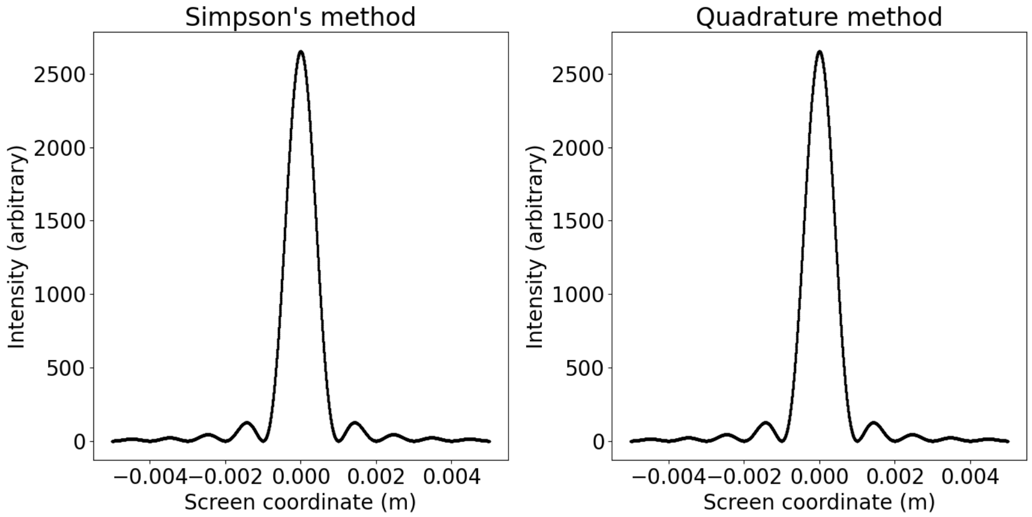

Figure 1. Far-field diffraction shown as light intensity as a function of screen coordinate. Left: Simpson's method for numerical integration. Right: quadrature method for numerical integration.

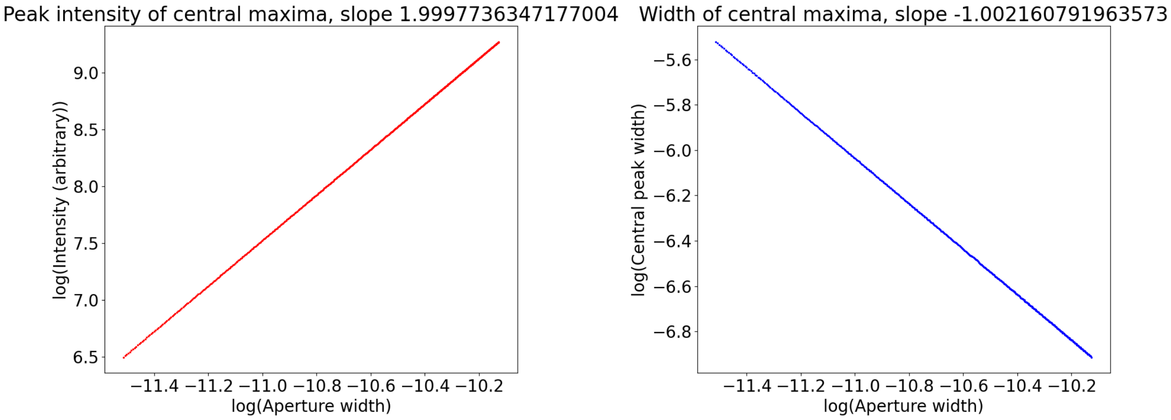

Figure 2. Left: log-log plot of central peak intensity as a function of aperture width. Right: log-log plot of central width as a function of aperture width.

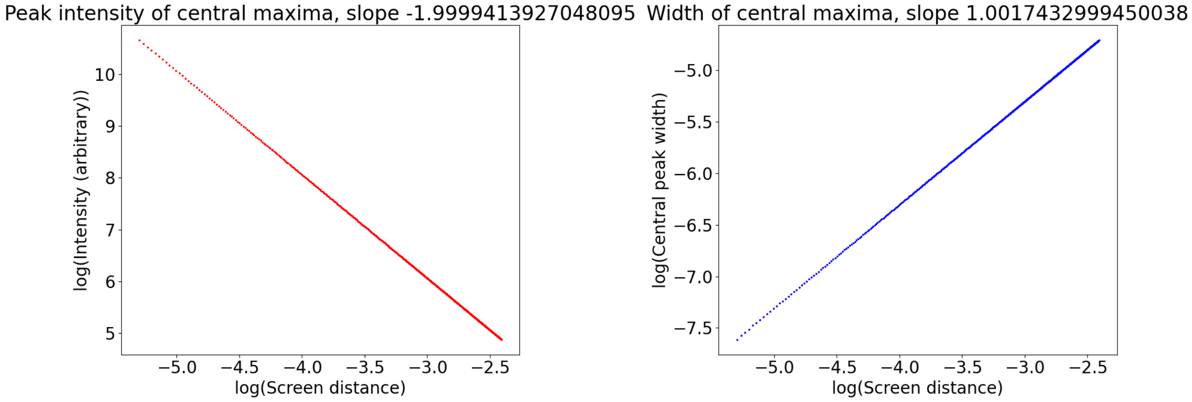

Figure 3. Left: log-log plot of central peak intensity as a function of screen distance. Right: log-log plot of central width as a function of screen distance.

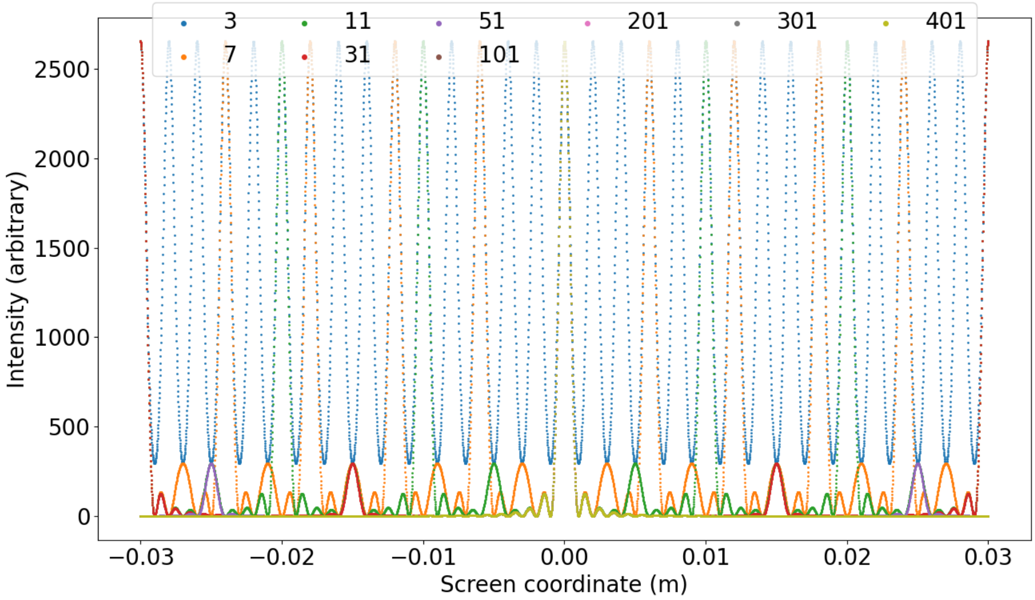

Figure 4. One dimensional far-field diffraction patterns at various sample sizes used in Simpson's numerical integration method, shown as light intensity as a function of screen coordinate.

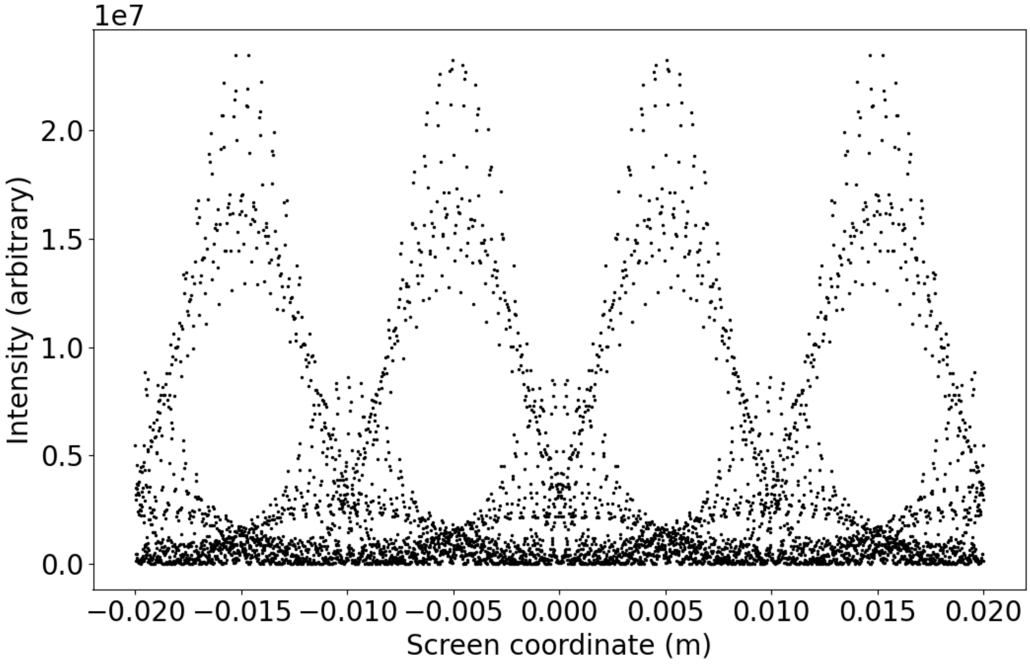

Figure 5. One dimensional near-field diffraction shown as light intensity as a function of screen coordinate.

observed. As expected, for z higher than this, the diffraction pattern becomes blurred and a 'central' bright 'circle' or 'oval' is seen instead as there is a loss in resolution at this distance. Fainter peaks can be seen in both approximations, similar to the 1-dimensional scenarios.

For part (d), limits were modified on the inner integral to change the aperture into a circle, and the results (Fig. 9) display near-field diffractions for z below $7.5 \times 10^{-5}\,\mathrm{m}$. An interesting phenomenon is observed—there can be a dark or low intensity spot at the centre, instead of a central maximum. This means that there is some

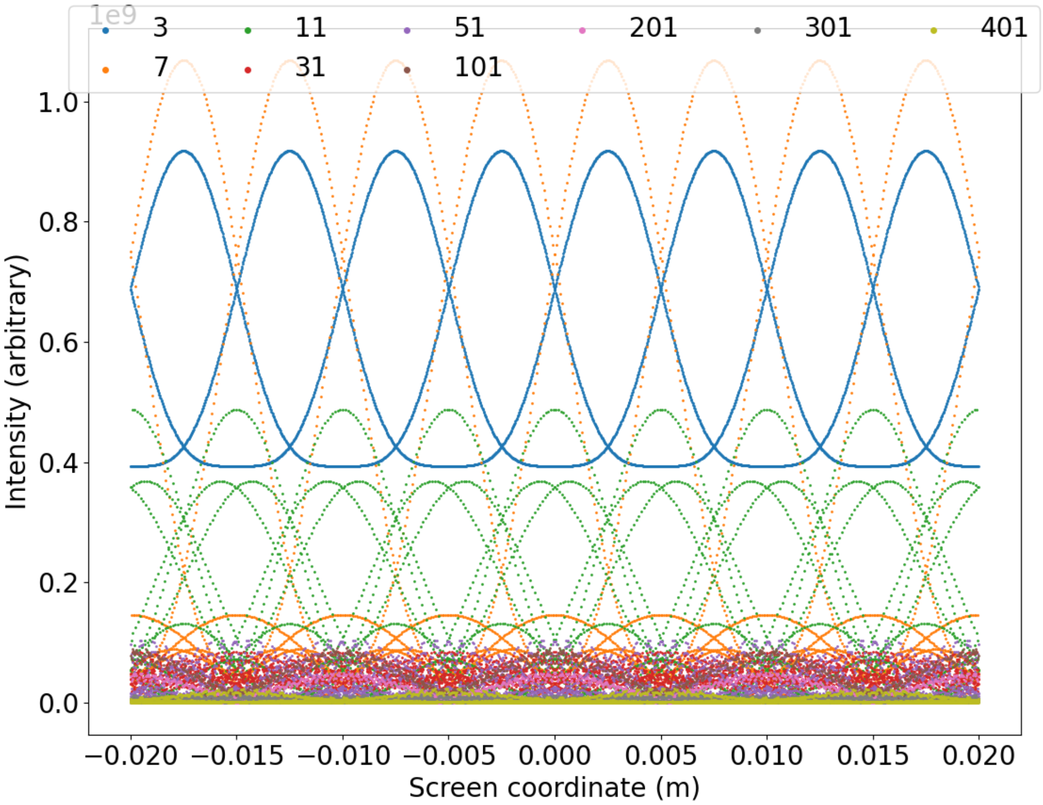

Figure 6. One dimensional near-field diffraction patterns at various sample sizes used in Simpson's numerical integration method, shown as light intensity as a function of screen coordinate.

phase destruction occurring here. In the far-field approximation, there is always a central maximum. This behaviour is characterised by the Fresnel number, F, where $F = R^2/z\lambda$. For even F (integer), a central minimum is observed, for odd F (integer), a central maximum is observed, F (non-integer) will be in-between minimum and maximum intensity [1]. For the top left aperture, $F = 13.\dot{3}$, so in-between bright and dark, and for the top right aperture, $F = 8$, predicting a complete minimum, which is observed. Some artefacts were also produced in the top left simulation, indicating some fine-tuning needed to be done with the parameters being passed into `scipy.integrate.dblquad()`.

E. Conclusion

One-dimensional and two-dimensional diffraction patterns were generated, both in the near-field regime and the far-field regime. The distinction between these two regimes were decided qualitatively (visually). Several physical phenomena were modelled with results as expected, namely the relationships of d_a and z with I_0 (central intensity) and 2θ (central width). Additionally, for the Simpson's integration method, a lower sample size was needed to accurately model far-field diffraction compared to near-field diffraction.

II. PROBLEM 2: MONTE CARLO INTEGRATION

A. Introduction

Problem 2 involved solving integrals using the Monte Carlo method. The situation is to find the "volume" of an n-dimensional sphere, for 2 to 10 dimensions.

Part (e) asked to evaluate a 2-dimensional integral using the Monte Carlo approach to find the area of a unit circle. Part (f) asked to investigate the error of the Monte Carlo method as a function of the sample size N for the previous calculation. Part (g) asked to extend the method onto higher dimensions up to 10 to find the volumes of the unit-hyperspheres.

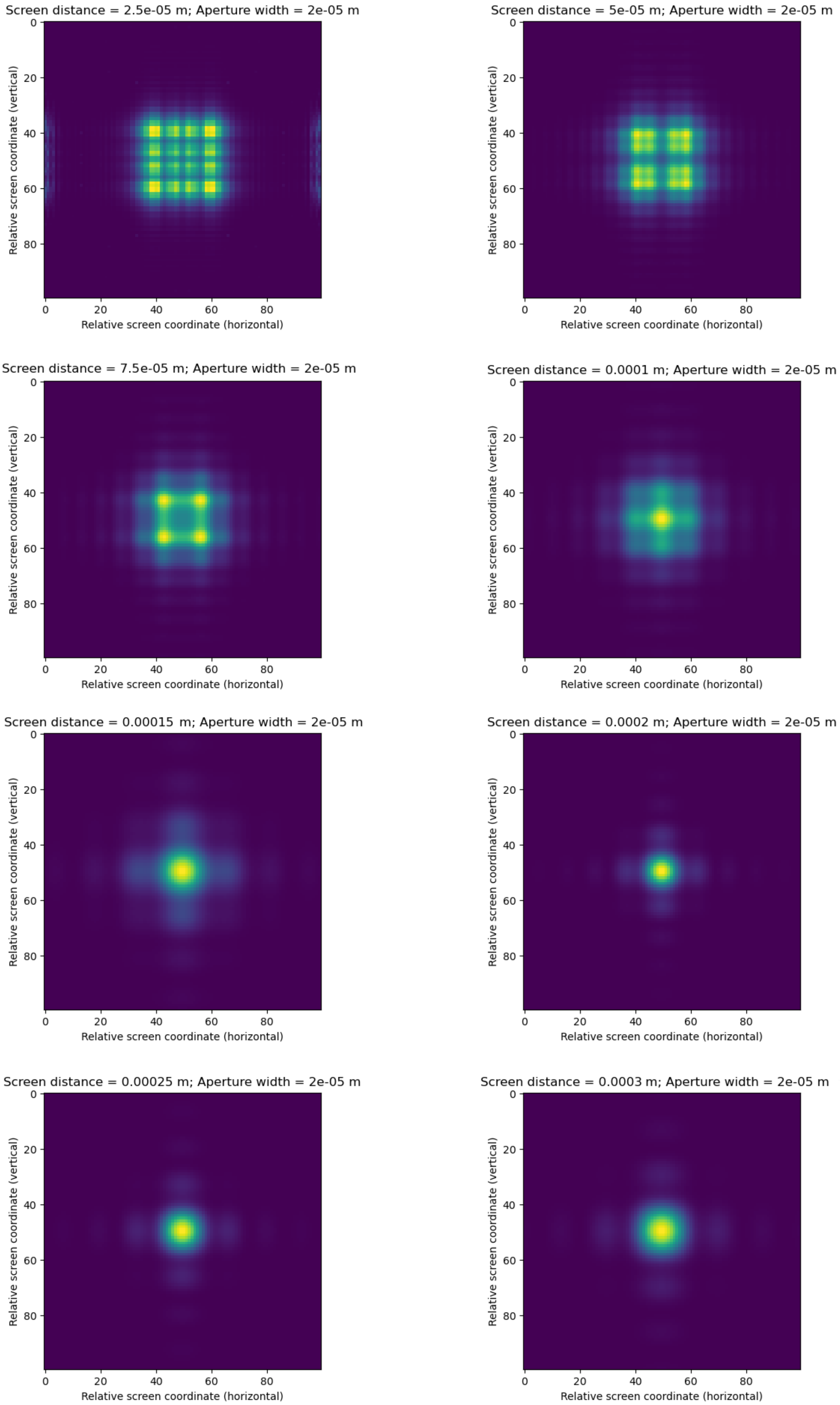

Figure 7. Two-dimensional diffraction through a square aperture for various screen distances.

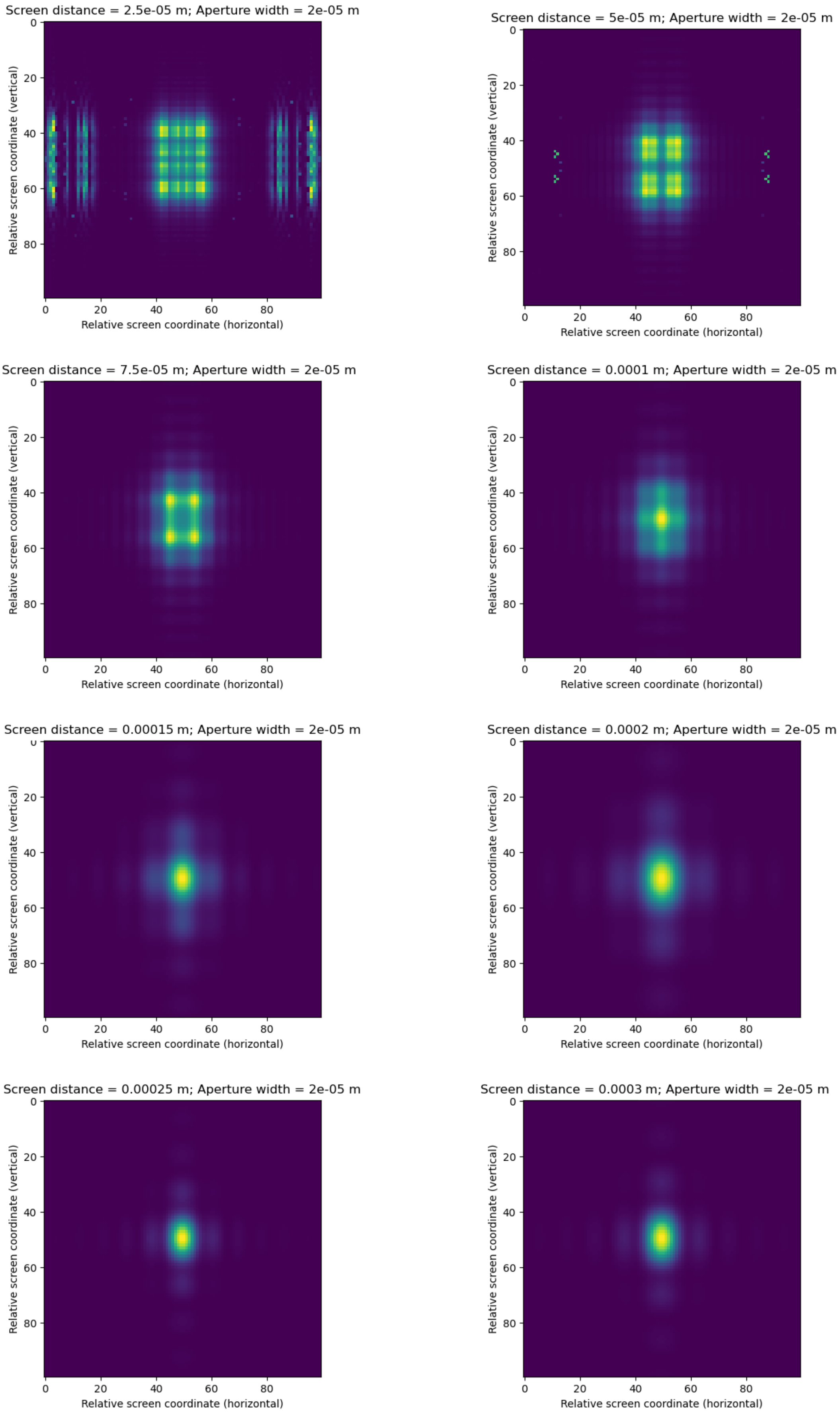

Figure 8. Two-dimensional diffraction through a rectangular aperture for various screen distances.

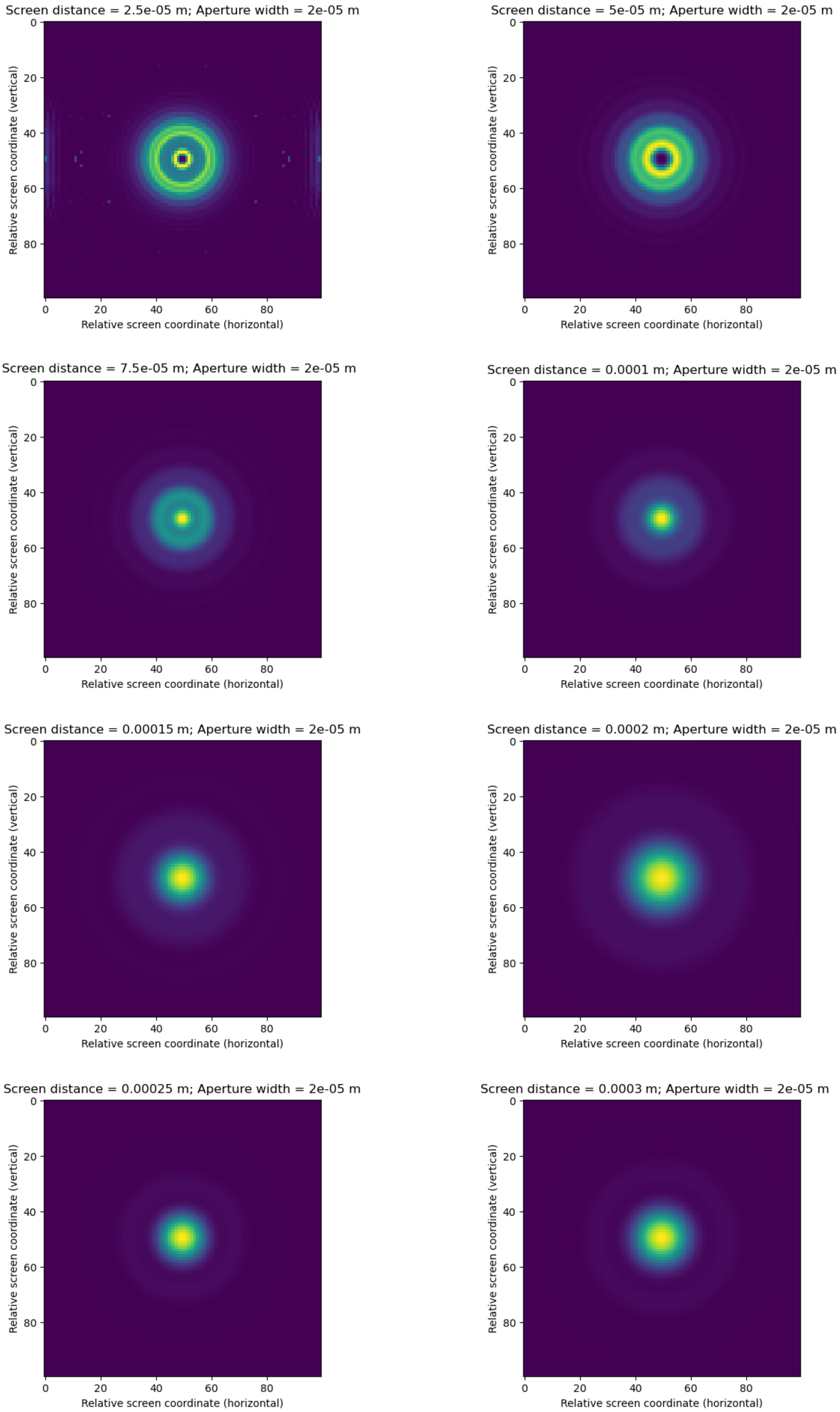

Screen distance = 2.5e-05 m; Aperture width = 2e-05 m

Screen distance = 5e-05 m; Aperture width = 2e-05 m

Screen distance = 7.5e-05 m; Aperture width = 2e-05 m

Screen distance = 0.0001 m; Aperture width = 2e-05 m

Screen distance = 0.00015 m; Aperture width = 2e-05 m

Screen distance = 0.0002 m; Aperture width = 2e-05 m

Screen distance = 0.00025 m; Aperture width = 2e-05 m

Screen distance = 0.0003 m; Aperture width = 2e-05 m

Relative screen coordinate (vertical)
0
20
40
60
80
Relative screen coordinate (horizontal)

Figure 9. Two-dimensional diffraction through a circular aperture for various screen distances.

B. Theory

The Monte Carlo method for solving integrals involves a sample of random numbers to sample the shape or function of the region to be integrated. The general equation is:

$$\int f \, \mathrm{d}V \approx V \left(\langle f \rangle \pm \sqrt{\frac{\langle f^2 \rangle - \langle f \rangle^2}{N}} \right) \tag{3}$$

The volume of a hypersphere of d-dimension is analytically given by:

$$V_d = \frac{2\pi r^2}{d} V_{d-2} \tag{4}$$

C. Method

For part (e), the area of a unit circle can be found using the Monte Carlo method. To constrain the samples to be within the circle, random numbers were generated within a square, then the function f in Eq. 3 simply return 0 if it lies outside the circle, or 1 if it lies inside.

For part (f), the convergence of the result is investigated. For a unit circle, the area is π. The sample number N was varied and its effects on the error was calculated.

For part (g), similar methods from part (e) and (f) were used to calculate the volume and the effect of N on the errors for hyperspheres up to 10 dimensions.

D. Results and discussions

For part (e), the Monte Carlo method was performed with $N = 500,000$. This typically yields an area of 3.14 ± 0.00164 unit area to 3 significant figures. Thus, it can obtain π to 2 decimal places.

For part (f), Fig. 10 shows 9,999 points generated for N from 50 to 500,000 (in increments of 50). On the left of the figure shows the convergence of results as the sample size increases. As seen on the right of the figure, the logarithm of the error decreases linearly with the logarithm of N. Modelling the relationship between error and N as Error $\propto N^p$, taking the logarithm of both error and N, and running a least squares linear fit using `numpy.polyfit` reveals the power p as the slope. In the 2D case, the slope was found to be -0.5, which means the error of the Monte Carlo method varies with $1/\sqrt{N}$. This statistical model works as expected and verifies Eq. 3.

Dimension d	Power p
1	-0.500
2	-0.500
3	-0.500
4	-0.500
5	-0.500
6	-0.500
7	-0.499
8	-0.500
9	-0.499
10	-0.497

Table II. The gradient of log-log plots to estimate the relationship between the errors of Monte Carlo integration and sample size.

For part (g), the method was generalised up to 10 dimensions. The convergence of results with N is shown in Fig. 11, along with the absolute errors in Fig. 12 (these plots are not contained within the submitted code). Results converge towards the true value as N increases for all dimensions tested. The difference in rates of convergence between each dimension is not clear from Fig. 11. The reason is because for some calculations, the volume ended up far from the true value, while for another dimension this might not have happened. This made each plot scale differently, so looking at all plots holistically, there is no pattern.

Similar to the method in 2 dimensions, logarithmic error was plotted against logarithmic N, as seen in Fig. 13. For each dimension, the slope of the logarithmic plot is approximated to be -0.5 to 1 significant figure, the table of all values is given in Table II. This indicates the errors vary with $1/\sqrt{N}$ in all dimensions up to 10. Looking at these plots holistically, it can be observed that the errors for higher dimensions appear to correlate worse as the number of dimensions increase, since the left 'tail' of the plot streamlines into a straight line slower.

One reason this could happen is the following: assuming the sample size N is now kept constant, as the number of dimensions d increases, the volume of the hypersphere decreases towards 0 very quickly (see Fig. 14), while the volume of the hypercube which contains the hypersphere increases ($V_\mathrm{d} = 2^d$ for a unit hypersphere). The result of this is the fraction of N that lies within the hypersphere $n_\mathrm{inside}/n_\mathrm{total}$ decreases as the d increases. While for any population of random variable, at large N, the central limit theorem shows that the population is distributed normally. At low N, the mean and variance is more sensitive to specific values. At higher d, at low values of N, there might not be enough data points within the hypersphere due to the fraction $n_\mathrm{inside}/n_\mathrm{total}$ being small compared to values at lower d, perturbing the sample standard deviation from the true population stan-

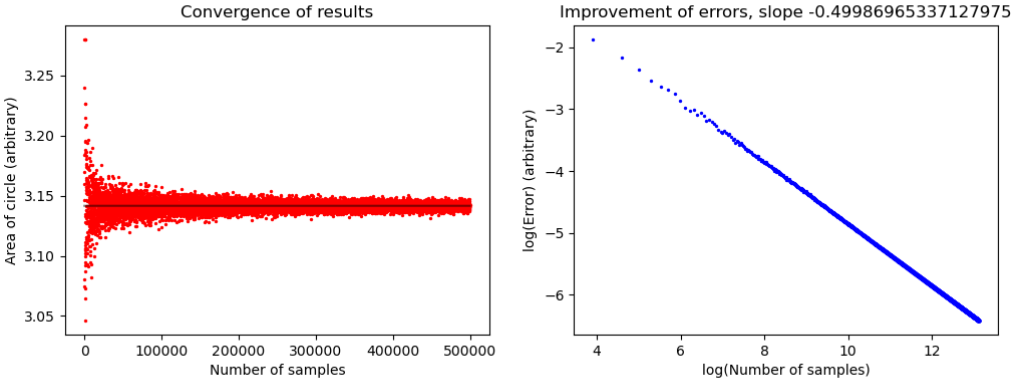

Figure 10. Left: results of Monte Carlo integration as a function of sample size to estimate area of a two-dimensional circle. Right: log-log plot of errors of integration versus sample size.

dard deviation. This leads to more perturbation is observed in the error (which is proportional to the standard deviation) at lower values of $\log N$ as d increases.

The Monte Carlo method utilised in part (e), (f), and (g) uses a pseudorandom number generator (PRNGs). PRNGs are not *truly random* as they are not unpredictable. Instead, they only approximate a sequence of *truly random* numbers, and remain deterministic by nature [2]. There are many methods to generate pseudorandom numbers, they tend to begin with an initial value—a seed. This seed can be obtained truly randomly, however, the algorithms that can be used to generate the numbers after the seed are deterministic.

However, a disadvantage of PRNGs as a sampler in Monte Carlo integration is that it might not cover the domain of interests thoroughly (all points might not be equidistributed inside the hypercubes). Instead, quasirandom number generators (Quasi-RNGs), which is less random than PRNGs, actually perform better than PRNGs in terms of quicker convergence. This method is known as the quasi-Monte Carlo method [3]. The Quasi-RNGs produce numbers with *low-discrepancy* [4]. A sample of numbers are *equidistributed* if the discrepancy tends to 0 as the sample size N goes to infinity [5]. An additional part (h) of this problem was added which used the `scipy.qmc.stats` library to generate a low-discrepancy sample of points, and the convergence comparison between the two is given by Fig. 15. A total of 35,000 integrations were performed, 5,000 at each N value to find the area of a circle. It can be seen that for both methods, the spread of values is on average centred around the true value π, but the spread of the quasi-Monte Carlo method is in all cases lower than the pseudorandom Monte Carlo method, indicating that convergence happens quicker as the density of results near the actual value at any given N is higher for the quasi-Monte Carlo than the pseudorandom Monte Carlo method.

E. Conclusion

The Monte Carlo method was used to approximate the volumes of hyperspheres for 2 to 10 dimensions. The method shows converge towards the actual value for all dimensions, and the error of the method is shown to vary with the inverse square root of the sample size. As one goes to higher dimensions, the ratio of points within the hypersphere to points outside the hypersphere decreases, meaning that at low values of N, the error (standard deviation) is perturbed from the sample standard deviation. In general, this is the pseudorandom Monte Carlo method, and it was qualitatively shown to converge more slowly than the quasi-Monte Carlo method.

[1] "Fresnel diffraction". Wikipedia. Retrieved 2023-02-12.

[2] "Pseudorandom number generators". Khan Academy. Retrieved 2023-02-12.

[3] "Equidistributed sequence". Wikipedia. Retrieved 2023-02-12

[4] "Low-discrepancy sequence". Wikipedia. Retrieved 2023-02-12.

[5] "Equidistributed sequence". Wikipedia. Retrieved 2023-02-12

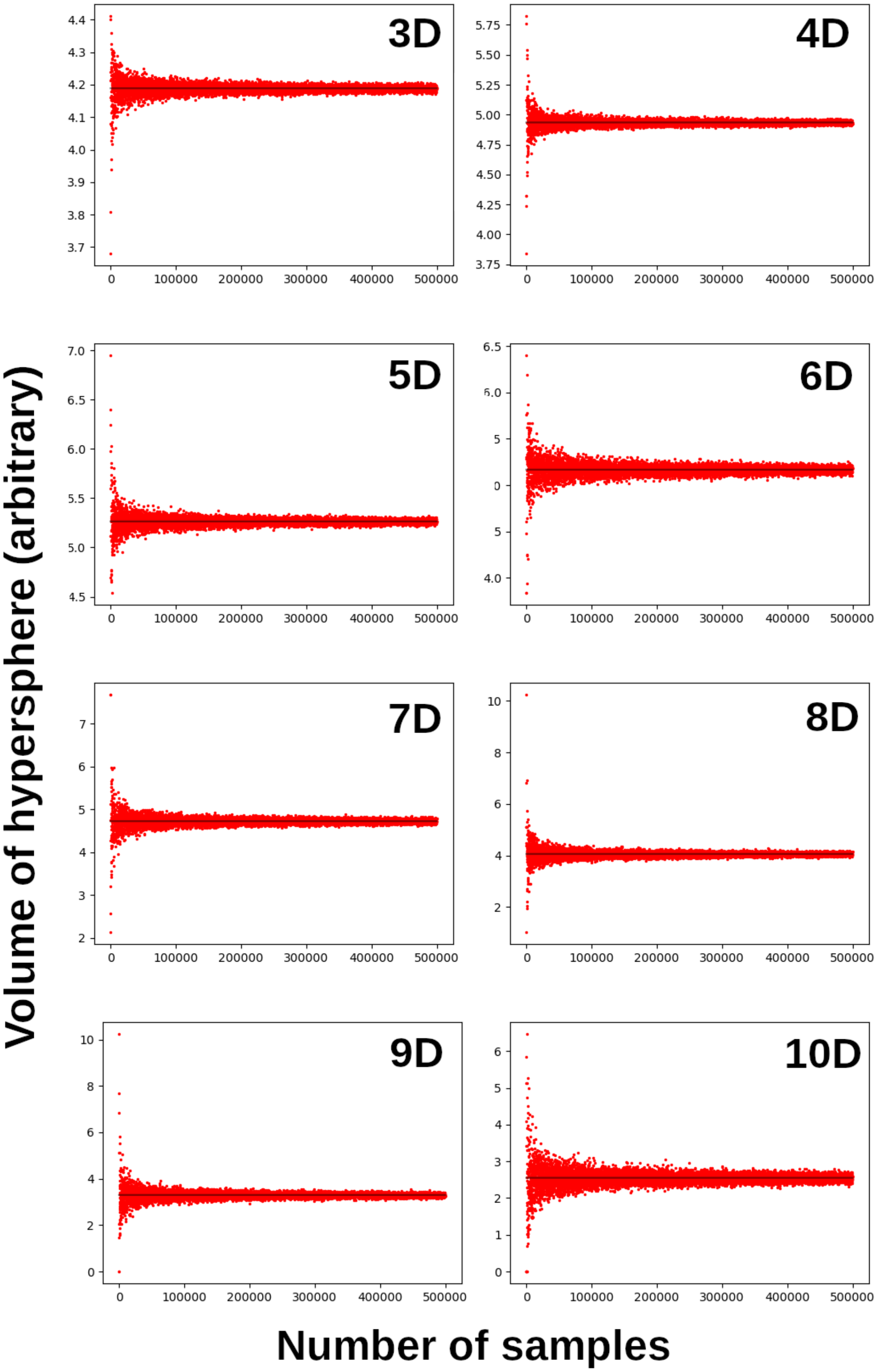

Figure 11. The results of Monte Carlo integration as a function of sample size for number of dimensions d from 3 to 10. The grey horizontal lines indicate the true value of convergence.

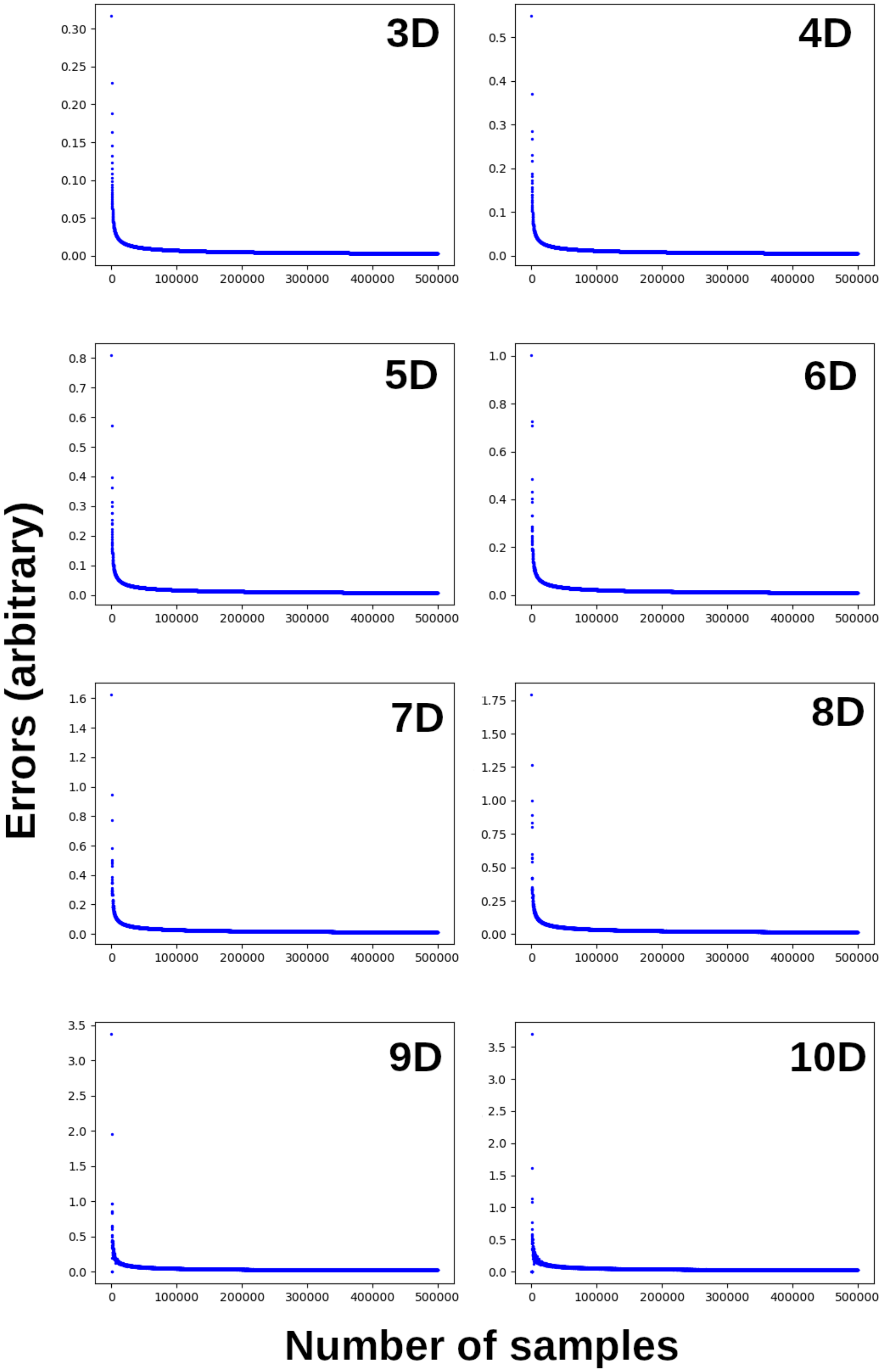

Figure 12. The absolute of errors of Monte Carlo integration as a function of sample size for number of dimensions d from 3 to 10.

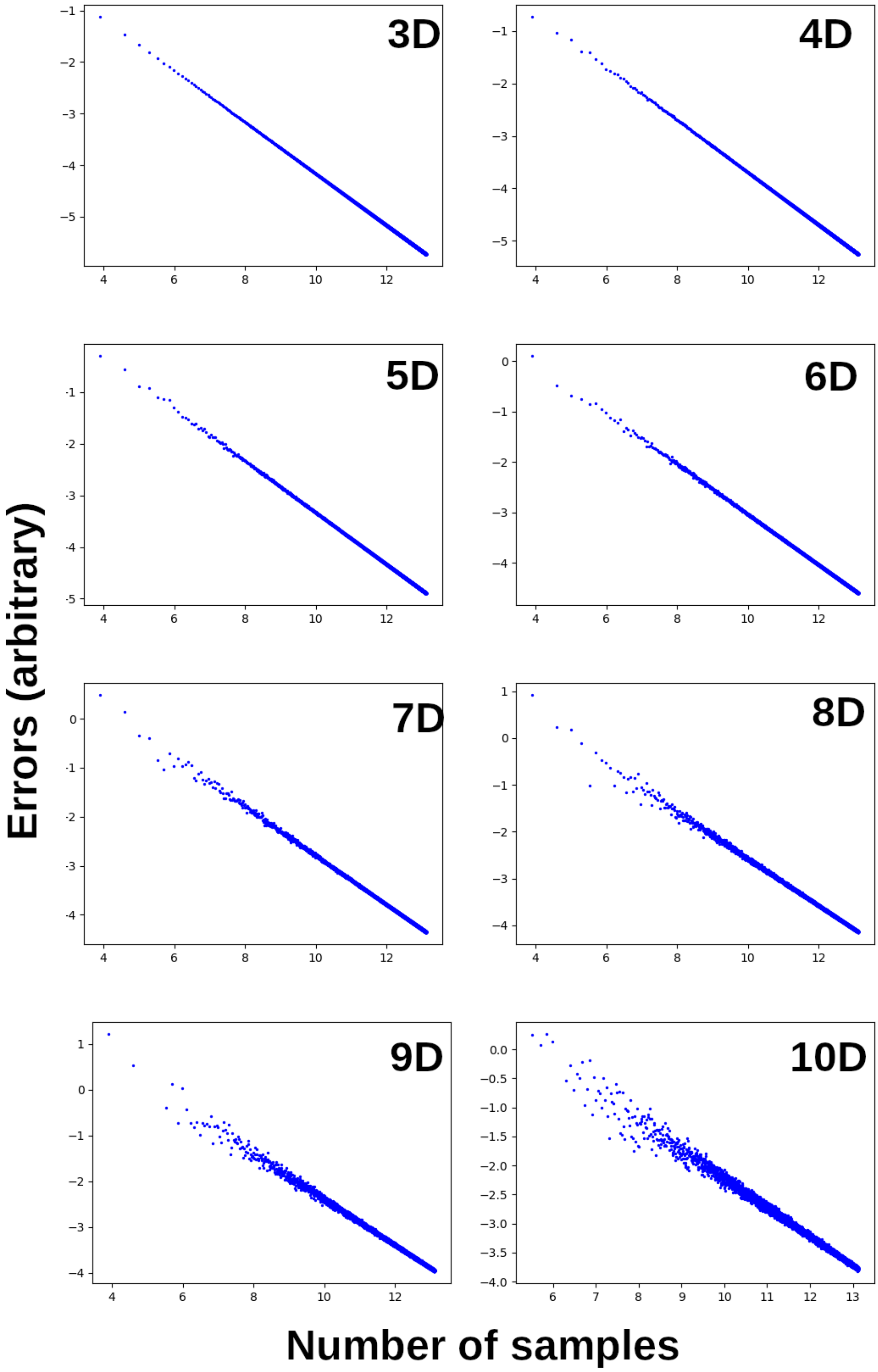

Figure 13. The log-log plot of errors of Monte Carlo integration versus sample size for number of dimensions d from 3 to 10.

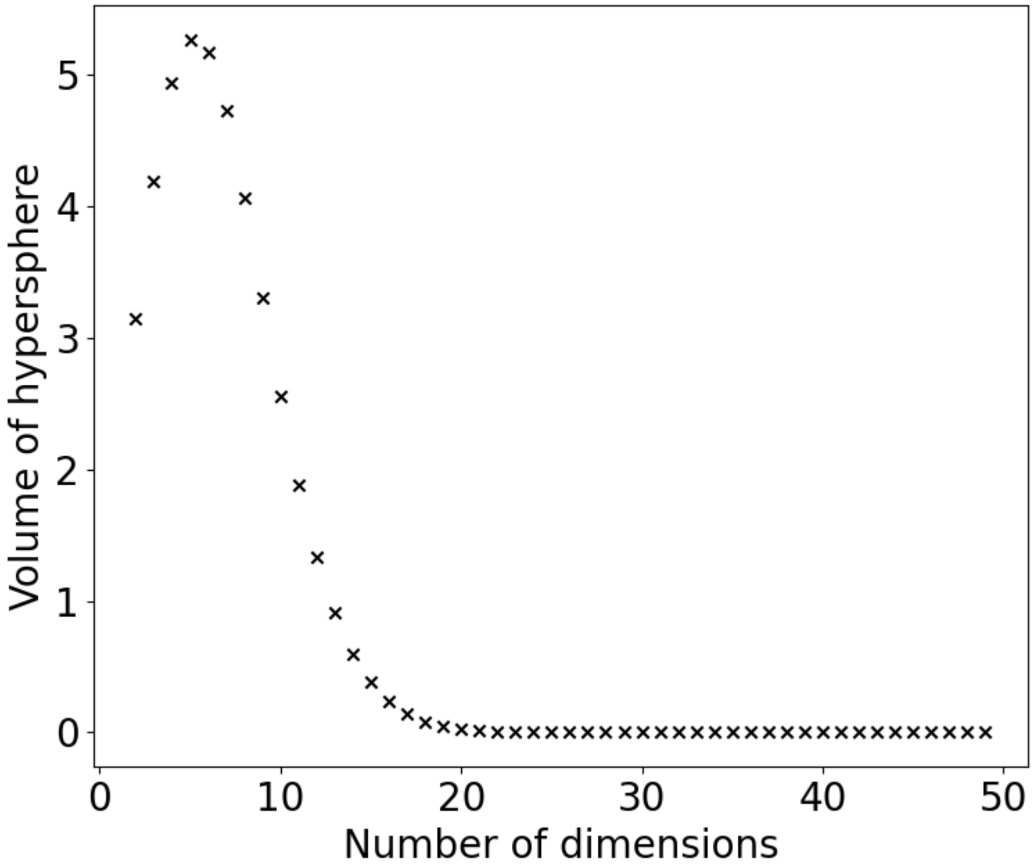

Figure 14. The volume of an n-ball or hypersphere as a function of the number of dimensions d. The peak value is at $d = 5$.

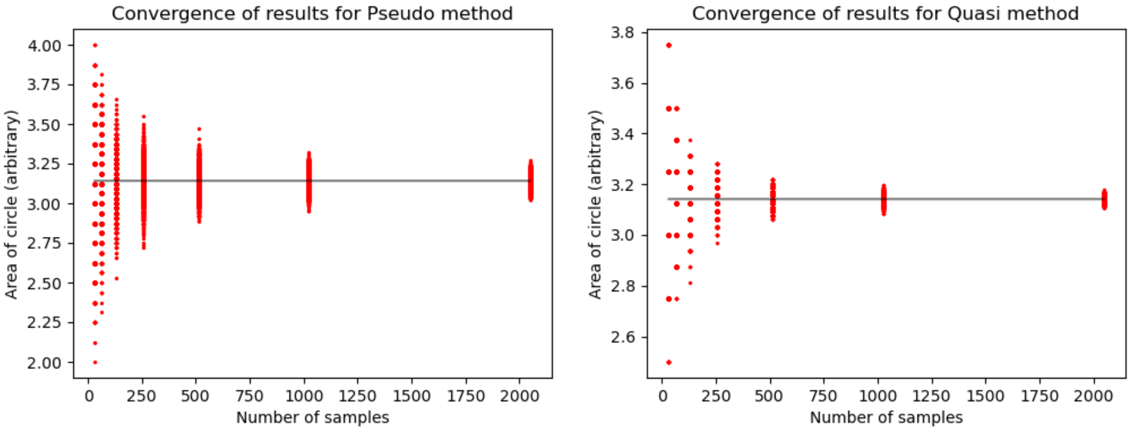

Figure 15. Comparison between convergence Pseudo-Monte Carlo (left) and Quasi-Monte Carlo (right). Grey horizontal line indicates the actual value.